# Electronic Supporting Information (ESI)

## Four-in-one multifunctional iron(III) complex for cancer theranostics: unique integration of targeted delivery, photodynamic therapy, and dual imaging modalities

Tukki Sarkar,*[a] Serena Rizzuti,[b†] Isorchand Chongtham,[b†] Rajesh Kushwaha,[c] Arnab Bhattacharyya,*[d] Samya Banerjee,*[c] Eliana Gianolio,*[b] Akhtar Hussain*[e]

**Author Affiliations**

[a] Tukki Sarkar
Department of Fluoro-Agrochemicals
CSIR-Indian Institute of Chemical Technology, Hyderabad 500007, Telangana, India

[b] Serena Rizzuti, Isorchand Chongtham, Prof. Eliana Gianolio
Department of Molecular Biotechnology and Health Sciences
University of Torino
Torino 10126, Italy.

[c] Rajesh Kushwaha, Dr. Samya Banerjee
Department of Chemistry, Indian Institute of Technology (BHU), Varanasi, Uttar Pradesh 221005, India

[d] Arnab Bhattacharyya
School of Chemistry, University of Birmingham, Birmingham B15 2TT United Kingdom.

[e] Akhtar Hussain
Department of Chemistry
Handique Girls' College, Guwahati 781001, Assam, India

[†] These authors contributed equally to the work

**Corresponding Authors**

Tukki Sarkar−Email: tukkisarkar11@gmail.com
Arnab Bhattacharyya−Email: a.bhattacharyya.1@bham.ac.uk
Samya Banerjee−Email: samya.chy@itbhu.ac.in
Eliana Gianolio−Email: eliana.gianolio@unito.it
Akhtar Hussain−Email: akhtariisc@gmail.com

## Experimental details

### Materials

Reagents and chemicals sourced from commercial suppliers (Sigma-Aldrich, U.S.A., TCI Chemicals Pvt. Ltd., and HiMEDIA, India) and used as received. Unless specifically stated, all solvents used in this research were purified and dried before use by standard methods.[1] Phosphate buffer saline (PBS) of pH 7.4 was prepared using deionized and double distilled water. Anhydrous $FeCl_3$, Dulbecco's Modified Eagle's medium (DMEM), esculetin (6,7-dihydroxycoumarin, 98%), *β*-D-glucose pentaacetate (98%), glutathione (GSH, > 98%), 4,6-O-ethylidene-*α*-D-glucose (EDG), 3-Fluoro-1,2-phenylene bis(3-hydroxybenzoate (WZB-117, > 98%), human serum albumin (HSA), methylene blue, Sodium azide, propidium iodide, 3-(4,5-dimethylthiazol-2-yl)-2,5-diphenyltetrazolium bromide (MTT), 9,10-anthracenediyl-bis(methylene)dimalonic acid (ABDA), 2',7'-dichlorofluorescein diacetate (DCFH-DA), 1,3-diphenylisobenzofuran (DPBF), Mitotracker Green (MTG), and Hoechst 33342 were procured from Sigma-Aldrich (U.S.A) and used as received. Annexin-V-FITC-PI kit (640914) for flow cytometry was procured from Invitrogen, U.S.A. Deferasirox was procured from Advanced Chemblocks Inc. Bis(2-pyridylmethyl)amine (di-2-picolylamine) was prepared as reported previously.[2] The glucose-conjugated ligand N,N-bis(2-pyridylmethyl)-2-aminoethyl-*β*-D-glucopyranoside (G-dpa) was prepared following a reported method (Ref. 47 in the manuscript). The phenyl-conjugated ligand bis-(2-pyridylmethyl)-benzylamine (P-dpa) was prepared by a previously published procedure.[3] Complex $[Fe(deferasirox)_2]^{3-}$ as its chloride salt (abbreviated $[Fe(DFX)_2]^{3-}$ in this work) was synthesized as described previously (Ref. 38 in the manuscript). Complexes $[Fe(CDTA)]^-$ and $[Fe(DTPA)]^{2-}$ were prepared as their meglumine salts for $^{17}O$-$R_2$-NMR experiments, following reported procedures (Ref. 36 in the manuscript).

### Methods

The elemental (CHN) analysis was performed by using a Thermo Finnigan Flash EA 1112 analyzer. The Fourier Transform (FT) infrared (IR) spectra were recorded using a Bruker ATR FT-IR spectrometer using powdered and dry samples. The UV-visible spectra of the complexes were recorded using a double-beam LABINDIA UV-visible spectrophotometer (Model: UV 3200). The solutions for the UV-visible measurements at 25°C were prepared in PBS (pH 7.4) or DMF/PBS (1:5 v/v, pH 7.4). Molar conductivity ($\Lambda_M$) was measured on an accurately calibrated Labtronics, India digital conductivity meter. Room temperature (25°C) magnetic susceptibilities were determined by a solution NMR method using DMSO-$d_6$ solutions of the complexes containing 1% TMS (v/v) as the internal reference and on a Bruker AMX-400 NMR spectrometer.[4] The magnetic moments were calculated by the Evans method using the equation: $\mu_{eff} = 0.0618(\Delta fT/fc)$, where $\Delta f$ is the observed shift in frequency of the TMS signal, $T$ is the temperature (K), $f$ is the operating frequency (MHz) of the NMR spectrometer, and $c$ is the molar concentration of the complex. The fluorescence spectra for complexes **Fe2** and **Fe3** were measured on a Shimadzu RF-6000 spectrofluorometer at 25°C. The deaerated solutions for the emission measurements were prepared in PBS (pH 7.4). Cyclic voltammetry (CV) experiments were performed on a Biologic SP-50 Potentiostat/Galvanostat (Biologic Instruments, France) consisting of a three-electrode setup with a platinum wire working electrode, platinum wire auxiliary electrode, and a standard KCl saturated calomel reference electrode (SCE). The scan speed was set at 100 $mVs^{-1}$. The

experiments were conducted using a 2.0 mM solution of the complexes prepared in DMF/PBS [9:1 (v/v)]. Tetrabutylammonium perchlorate (TBAP, 0.1 M) was the supporting electrolyte. Electrospray ionization high-resolution mass spectra (ESI-HRMS) were recorded on an Agilent Technologies 6538 UHDA-Quadruple-TOF LC/MS mass spectrometer using the positive (+) mode. Flow cytometric analysis was performed using FACS Calibur (Becton Dickinson (BD) cell analyzer) at FL1 channel (595 nm).

**Synthesis of the precursor complexes [Fe(G-dpa)$Cl_3$] and Fe(P-dpa)$Cl_3$]**

The precursor complexes [Fe(G-dpa)$Cl_3$] and Fe(P-dpa)$Cl_3$] were synthesized by general method in which anhydrous $FeCl_3$ (0.161 g, 1.0 mmol) was dissolved in anhydrous methanol (10 mL) followed by dropwise addition of a solution of G-dpa (0.405 g, 1.0 mmol) or P-dpa (0.289 g, 1.0 mmol) prepared in anhydrous methanol (10 mL). The solution was stirred at room temperature for 2 hours during which a light yellow solid precipitated. The solid was filtered, washed with ice-cold ethanol (10 × 2 mL) followed by diethyl ether ( 10 × 2 mL), and finally dried in a vacuum overnight using $P_4O_{10}$ as the desiccant. The precursor complexes were then used in the next synthetic step. The identity and purity of the synthesized precursors were confirmed through elemental CHN analysis.

**[Fe(G-dpa)$Cl_3$]:** Yield: ~50%. Anal. Calcd for $C_{20}H_{27}N_3O_6Cl_3Fe$: C, 42.32; H, 4.79; N, 7.40 Found: C, 42.48; H, 4.78; N, 7.38.

**Fe(P-dpa)$Cl_3$]:** Yield: ~65%. Anal. Calcd for $C_{19}H_{19}N_3Cl_3Fe$: C, 50.53; H, 4.24; N, 9.31 Found: C, 50.71; H, 4.25; N, 9.28.

**Synthesis of complexes Fe1–Fe3**

Complexes **Fe1**–**Fe3** were synthesized by a general method in which the precursor complex [Fe(G-dpa)$Cl_3$] (0.283 g, 0.5 mmol) or [Fe(P-dpa)$Cl_3$] (0.225 g, 0.5 mol) was suspended in anhydrous methanol ( 10 ml). To this suspension, a solution of catechol ($H_2$cat, 0.055 g, 0.5 mmol) or esculetin ($H_2$esc, 0.089 g, 0.5 mmol) in anhydrous methanol (10 mL) was added dropwise in the presence of 2 equivalents of triethylamine (0.101 g, 1.0 mmol). The reaction mixture immediately turned into a dark green solution and it was stirred at room temperature for 2 hours. The solution was then filtered and the volume of the solution was reduced to 10 mL at room temperature under reduced pressure using a rotary evaporator. Diethyl ether (20 mL) was added to the solution to induce the formation of a green precipitate, which was filtered and washed with diethyl ether ( 10 × 2 mL). The solid was dissolved in 5 mL of DMF and immediately reprecipitated by adding diethyl ether (30 mL) as a green solid. The solid was subsequently filtered, washed with diethyl ether ( 10 × 2 mL), and finally dried in a vacuum over $P_4O_{10}$.

**Characterization data**

**[Fe(G-dpa)(cat)Cl] (Fe1)**: % Yield: ~55. Calcd for $C_{26}H_{31}N_3O_8ClFe$: C, 51.63; H, 5.17; N, 6.95; Observed: C, 51.75; H, 5.16; N, 6.93. ESI-HRMS (*m/z*) in MeOH/$H_2O$ (19:1 v/v): Calculated for $[M+H]^+$ 605.1227, Observed 605.1245; Calculated for $[M–Cl]^+$ 569.1461, Observed 569.1483. FT–IR data ($cm^{-1}$): 3363 sbr, 2985 m, 2809 w, 2730 w, 1655 m, 1572 m, 1474 m, 1450 m, 1396 m, 1325 s, 1282 s, 1155 w, 1091 w, 1043 m, 1018 m, 900 w, 850 w, 793 w, 758 m, 701 w, 635 w, 611 w (sbr, strong broad; vs, very strong; s, strong; m, medium; w, weak). UV–visible in PBS [pH 7.4], [$\lambda_{max}$/nm ($\varepsilon$/$M^{-1}$ $cm^{-1}$)]: 270 (13,600), 353 sh (3,300), 735 (1,670). $\mu_{eff}$ = 5.83 B.M. at 298 K. Molar conductivity ($\Lambda_M$) in DMF at 25 °C [S $cm^2$ $mol^{-1}$]: 13.

**[Fe(G-dpa)(esc)Cl] (Fe2)**: % Yield: ~60. Calcd for $C_{29}H_{31}N_3O_{10}ClFe$: C, 51.76; H, 4.64; N, 6.24; Observed: C, 51.87; H, 4.65; N, 6.23. ESI-HRMS (*m/z*) in MeOH/$H_2O$ (19:1 v/v): Calculated for $[M+H]^+$ 673.1126, Observed 673.1141; Calculated for $[M–Cl]^+$ 637.1359, Observed 637.1377. FT–IR data ($cm^{-1}$): 3367 sbr, 2990 m, 2803 w, 2725 w, 1636 s, 1572 m, 1470 m, 1450 m, 1390 m, 1360 m, 1273 w, 1155 w, 1027 m, 895 w, 856 w, 836 w, 790 w, 758 w, 699 w, 636 w. UV–visible in PBS [pH 7.4], [$\lambda_{max}$/nm ($\varepsilon$/$M^{-1}$ $cm^{-1}$)]: 271 (18,000), 386 (14,800), 470 sh (4,170), 508 sh (3,300), 730 (3,650). $\mu_{eff}$ = 5.89 B.M. at 298 K. Molar conductivity ($\Lambda_M$) in DMF at 25 °C [S $cm^2$ $mol^{-1}$]: 18.

**[Fe(P-dpa)(esc)Cl] (Fe3)**: % Yield: ~51. Calcd for $C_{28}H_{23}N_3O_4ClFe$: C, 60.40; H, 4.16; N, 7.55; Observed: C, 60.65; H, 4.16; N, 7.53. ESI-HRMS (*m/z*) in MeOH/$H_2O$ (19:1 v/v): Calculated for $[M+H]^+$ 557.0805, Observed 557.0783; Calculated for $[M–Cl]^+$ 521.1038, Observed 569.1022. FT–IR data ($cm^{-1}$): 3074 w, 2983 w, 2791 w, 2700 w, 1665 s, 1598 m, 1578 s, 1537 m, 1476 s, 1436 s, 1386 s, 1355 m, 1285 s, 1264 s, 1174 m, 1163 m, 1133 w, 1093 w, 1052 w, 1022 m, 921 w, 850 w, 810 w, 760 w, 700 m, 638 w. UV–visible in PBS/DMF [5:1 v/v, pH 7.4], [$\lambda_{max}$/nm ($\varepsilon$/$M^{-1}$ $cm^{-1}$)]: 268 (15,400), 392 (12,100), 472 sh (3,750), 630 (2,500). $\mu_{eff}$ = 5.85 B.M. at 298 K. Molar conductivity ($\Lambda_M$) in DMF at 25 °C [S $cm^2$ $mol^{-1}$]: 23.

**Computational calculations**

The Fe(III) complexes (**Fe1**−**Fe3**) were prepared in GaussView 5 software and cleaned using the VSEPR theory. The DFT optimization of both complexes was carried out using the Gaussian16 software with a LANL2DZ basis set for Fe and 6-31g* for other atoms with the B3LYP function in vacuum.[5] The optimized structures were further characterized by harmonic vibrational frequency analysis to confirm that real local minima without any imaginary frequency were reached at the same computational level. The theoretical UV-visible spectra were determined in DMSO as a solvent utilizing the CPCM solvent model. The selected transitions were further calculated using Natural Transition Orbitals (NTO) analysis. Visualizations of the optimized structures and the frontier molecular orbitals (HOMOs and LUMOs) and NTO of the complexes were performed using the Gaussian 16 software. Time-dependent density functional theory (TDDFT) was used to calculate electronic transitions and transition probabilities in DMSO.

**Fluorescence quantum yield ($\Phi_f$) determination**

The fluorescence quantum yields of **Fe2** and **Fe3** were measured by using coumarin-153 laser dye as a reference, having a known quantum yield value of 0.56 in acetonitrile.[6] The sample for quantum yield determination was deoxygenated before spectral measurements. The sample and reference were excited at 430 nm, maintaining a low (< 0.1) but nearly equal absorbance. The integrated emission intensity was calculated using Origin 2022 software and the quantum yield was calculated using the equation $\Phi_f/\Phi_R = (A_f/A_R) \times [(OD)_R/(OD)_f] \times [(n_f)^2/(n_R)^2]$, where, $\Phi_f$ and $\Phi_R$ are the fluorescence quantum yields of the sample and reference respectively, $A_f$ and $A_R$ are the area under the fluorescence spectra of the sample and the reference respectively, $(OD)_S$ and $(OD)_R$ are the respective optical densities of the sample and the reference solution at the wavelength of excitation, and $n_f$ and $n_R$ are the respective refractive indices of the solvents used for the sample and the reference.[7]

**Lipophilicity determination**

The lipophilicity of the complexes was measured by determining their partition coefficients (log $P_{o/w}$) between *n*-octanol (o) and water (w) using the shake-flask method.[8] A calibration plot for the complex was constructed by determining the absorbances by varying concentrations of the complex in the aqueous medium. Then, the known concentration of the aqueous solution of the complex was mixed with an equal volume of *n*-octanol. After vortex-shaking the mixture, the two phases were allowed to separate. The remaining concentration of the complex in the aqueous phase was then determined from the calibration plot. The partition coefficient was calculated by using the equation log $P_{o/w}$ = log $c_o/c_w$, where $c_o$ is the concentration of the complex in the *n*-octanol phase and $c_w$ is the concentration in the aqueous phase.

**Stability and photostability experiments**

UV-visible and emission spectroscopy were used to evaluate the thermodynamic stability of the complexes by recording the spectra at 25°C of a solution of **Fe2** prepared in PBS (pH 7.4). Reduced glutathione (GSH, 1.0 mM) was used as an additive for the stability assessment of **Fe2** in its presence. The photostability of the complexes was investigated by recording the UV-visible and emission spectra of a solution of **Fe2** prepared in PBS (pH 7.4) after irradiating the solution (every 10 minutes up to 1 hour) with a diode laser (705 nm, 38 mW, Newport Corporation, U.S.A.).

**Cell culture**

HeLa (human cervical carcinoma), MCF-7 (human breast adenocarcinoma), and MCF-10A (human breast epithelial) cell lines for monolayer cultures were obtained from the National Centre for Cell Science (NCCS), Pune, India, and American Type Culture Collection (ATCC), U.S.A. Cells were maintained in DMEM supplemented with 10% FBS, 100 IU $mL^{-1}$ of penicillin, 100 $\mu$g $mL^{-1}$ of streptomycin, and 2.0 mM of Glutamax at 37 °C in a humidified incubator at 5% $CO_2$. The adherent cultures were grown as monolayers and were maintained by trypsinizing with 0.25% Trypsin-0.2 % EDTA.

**Phototoxicity experiments**

Cytotoxicity of the complexes was studied by the colorimetric MTT [3-(4,5-dimethylthiazole-2-yl)2,5-diphenyltetrazolium bromide] assay, which is based on the ability of mitochondrial dehydrogenases of viable cells to cleave the tetrazolium rings of MTT, forming dark purple membrane-impermeable crystals of formazan that can be estimated from the spectral measurements in DMSO.[9] Stock solutions of the complexes were prepared in either Milli-Q water (for **Fe1** and **Fe2**) or DMSO (for **Fe3**) for cytotoxicity measurements and the percentage of DMSO used for **Fe3** in the culture media was within the permissible limit (up to 1%). Cells were added to a 96-well plate (~12,000 cells/well) and allowed to incubate overnight followed by dark incubation (2 or 4 hours as required) with the compound at varying concentrations. The medium was then replaced with PBS (pH 7.4) and cells were photo-irradiated with red light (600–720 nm, 50 J $cm^{-2}$, 15 minutes) delivered from a Waldman PDT 1200L (Germany) photoreactor. PBS was replaced with 10% DMEM after irradiation and cells were incubated for a further period of 20 h in the dark. Post incubation, 25 $\mu$L of MTT (4 mg $mL^{-1}$ in PBS) was added to each well

and incubated for an additional 3 hours. The culture medium was discarded and 200 µL of DMSO was added to solubilize the formazan crystals. The absorbance was measured at 540 nm using a Molecular Devices Spectra Max M5 plate reader. Cytotoxicity of the complexes was measured as the percentage ratio of the absorbance of the treated cells to the untreated controls. The cytotoxicity was expressed in terms of the $IC_{50}$ values which were determined by nonlinear regression analysis using GraphPad Prism software.

**Statistical analysis**

One-way analysis of variance (ANOVA) was performed to compare $IC_{50}$ values across different glucose concentrations (1.0 mM, 5.0 mM, and 10.0 mM). Post-hoc pairwise comparisons were conducted using Tukey's multiple comparisons test to identify significant differences between groups. A $p$-value < 0.05 was considered statistically significant. Results are presented as mean ± standard deviation (SD) from three independent experiments, each conducted in triplicate.

**Quantification of whole Cell Fe content by ICP-MS**

The quantification of **Fe2** and **Fe3** in HeLa, MCF-7, and MCF-10A cells was done by inductively coupled plasma-mass spectrometry (ICP-MS) analysis.[10] Approximately, 1 × $10^6$ cells were seeded in 60 mm culture dishes and treated with the complex (10 $\mu$M) in duplicate for 2 or 4 hours. The medium was discarded, and the cells were washed with PBS. The cells in one dish were digested with 0.5 mL hot conc. $HNO_3$ (~90 $^0$C) for ~2 h, diluted to 10 mL with 2% v/v $HNO_3$, and the amount of metal internalized into the cells (expressed as ng per $10^6$ cells) was quantified by ICP-MS technique. The live cells were counted by the trypan blue method after trypsinization. The uptake of Fe in the complex into the cells was calculated by subtracting the average Fe content of the control cells from that of complex-treated cells and normalizing to the average number of cells per well.

**Annexin-V FITC-propidium iodide assay**

HeLa cells (~ 3 × $10^5$ cells $mL^{-1}$) were treated with **Fe2** (15 $\mu$M) in 10% DMEM for 2 hours, followed by exposure to red light (600–720 nm, 50 J $cm^{-2}$, 15 minutes) delivered from a Waldman PDT 1200L (Germany) photoreactor. The cells were then post-incubated in the dark for an additional 2 hours. The medium was then discarded, and cells were harvested and washed twice with chilled PBS at 4°C. The cells were re-suspended in 100 $\mu$L Annexin-V binding buffer (100 mmol HEPES/ NaOH, pH = 7.4 containing 140 mmol NaCl and 2.5 mmol $CaCl_2$), stained with Annexin-V FITC (2 $\mu$L) and propidium iodide (5 $\mu$L), and incubated for 15 minutes at room temperature in the dark. After incubation, 400 $\mu$L of binding buffer was added to the cells and analyzed immediately using flow cytometry.[11]

**ROS generation**

HeLa cells (~ 2 × $10^5$ cells $mL^{-1}$) were treated with **Fe2** (15 $\mu$M) in 10% DMEM for 2 hours. After harvesting, 10 $\mu$L of DCFDA stock solution (1.0 mM) in 100 $\mu$L of PBS was added to the cells and incubated for 20 mins. The sample was irradiated with (600–720 nm, 50 J $cm^{-2}$, 15 minutes) delivered from a Waldman PDT 1200L (Germany) photoreactor. The formation of ROS was monitored by recording the intensity of DCF (formed by oxidation of DCFDA) at 525 nm in the FITC channel.[12] 9,10-anthracenediylbis(methylene)dimalonic acid (ABDA) was used as a probe for detecting the formation

of any singlet oxygen ($^1O_2$) by **Fe2** under red laser light (705 nm, 38 mW, Newport Corporation, U.S.A.) irradiation (Ref. 56 in the manuscript). A stock solution (1.0 mM) of **Fe2** was prepared in water and added to the ABDA (1.0 mM) stock solution in water to obtain a final concentration of 12 $\mu$M of ABDA and 20 $\mu$M of **Fe2**. The decrease in absorbance of the anthracene-centered band of ABDA at 378 nm was monitored at an interval of 1 minute of continuous irradiation with red light and monitored for up to 10 minutes (705 nm, 38 mW). To study the effect of quenching, $NaN_3$ (10.0 mM) was used as a known $^1O_2$ quencher. For experiments to detect hydroxyl radical (HO•) generation, disodium terephthalate (TA) at a final concentration of 30 $\mu$M was used. For the HO• radical scavenging experiment, KI (2.0 mM) was used as a known scavenger.

**Singlet oxygen quantum yield ($\Phi_\Delta$) measurement**

The singlet oxygen quantum yields for **Fe2** and **Fe3** were determined through a titration experiment using 1,3-diphenylisobenzofuran (DPBF). DPBF is a well-known quencher for singlet oxygen, reacting with it to produce 1,2-dibenzoylbenzene. DPBF and complex (**Fe2** or **Fe3**) were dissolved in DMSO at a molar ratio of 60:1 and exposed to red light (705 nm, 38 mW). The photooxidation of DPBF was monitored by measuring the decrease in absorbance at 417 nm at an interval of 5 s. To determine the quantum yield, methylene blue (MB, $\Phi_\Delta$ = 0.52) was employed as a standard. The decrease in intensity of the absorption maxima of DPBF at approximately 417 nm was plotted against the irradiation time. The singlet oxygen quantum yield values ($\Phi_\Delta$) were obtained by using the following equation,

$$\Phi_{\Delta c} = \Phi_{\Delta MB} \times (m_c/m_{MB}) \times (F_{MB}/F_c)$$

Where "*c*" refers to complex and "MB" refers to methylene blue, $\Phi_\Delta$ is the value of singlet oxygen quantum yield, *m* is the slope of ΔOD vs. time (s) plot and *F* is the absorption correction factor, defined as $F = 1-10^{-OD}$, where OD is the optical density (absorbance) at the irradiation wavelength (Ref. 57 in the manuscript).

**Optical imaging**

The cellular localization of **Fe2** was studied using confocal fluorescence microscopy. HeLa and MCF-7 cells (~ $6 \times 10^4$) were cultured overnight in Thermo Scientific Nunc 35 mm glass bottom dishes using 10% FBS-DMEM medium. The cells were then incubated with **Fe2** (5 $\mu$M) for 2 hours, and the culture medium was replaced with fresh medium. Mitotracker Green (MTG, 200 $\mu$L of 250 nM stock in PBS buffer of pH 7.4) was then added to the dishes and incubated for 15 minutes. Nucleus targeting Hoechst 33342 dye (5 $\mu$L from 1 $\mu$g/mL stock in PBS buffer, pH 7.4) was also added to the cells and incubated for ~10 minutes. The trackers were then washed with PBS, and the culture medium was also replaced with PBS buffer. Finally, confocal microscopic experiments were performed using an Olympus FV 3000 confocal microscope at 60× magnification. To record the emission of **Fe2** (displayed as red), the sample was excited using a 405 nm blue laser light source. The acquired images were then processed using Olympus cellSens imaging software (Ref. 21 in the manuscript). The Pearson Coefficient (PC) and Operlap Coefficient (OC) for confocal images were calculated using ImageJ software with the JACoP plugin.

**Relaxometric experiments**

Observed longitudinal relaxation rates ($R_{1obs} = 1/T_{1obs}$) values were measured by inversion recovery at 21.5 MHz and 25 °C using a Stelar SpinMaster spectrometer (Stelar s.r.l, Mede (PV), Italy). The temperature was controlled with a Stelar VTC-91 airflow heater and checked with a calibrated RS PRO RS55-11 digital thermometer. Data were determined using a recovery time of ≥ 5 × $T_1$ (2 scans per data point). The absolute error in $R_{1obs}$ measurements was less than 1%.

According to a procedure previously reported in the literature[13], the Fe(III) concentrations were obtained by mixing the complex solutions (**Fe1** or **Fe2**) in a 1:10 v/v ratio with 69% $HNO_3$ and heating in sealed vials at 120 °C overnight to yield a solution of $Fe^{3+}$ aqua ion. The $R_{1obs}$ of the solution was measured at 25 °C and 21.5 MHz and the concentration was determined using the equation $R_{1obs} = R_{1d} + r_{1p}^{Fe}$ [Fe], where $R_{1d}$ is the diamagnetic contribution (0.48 $s^{-1}$) and $r_{1p}^{Fe}$ is the $Fe^{3+}$ aqua ion relaxivity (18.47 $mM^{-1}$ $s^{-1}$) under the same experimental conditions. ICP-MS analysis confirmed the Fe concentration of the complexes.

Longitudinal relaxivity ($r_1$) values reported in Table 2a were calculated as the slope of the lines correlating observed relaxation rates measured at a pH of 7.4, 25 °C, or 37 °C, and 0.47 T as a function of complex concentration.

Stability experiments were performed measuring the $R_{1obs}$ values at 25 °C and 21.5 MHz over 3 hours, while the PBS (pH 7.4) and HSA solutions of the complex were stored in sealed tubes at 37 °C.

The interaction of the complex (**Fe1** or **Fe2**) with HSA was investigated using the proton relaxation enhancement (PRE) method, as reported by us previously (Ref. 38 in the manuscript). Briefly, the apparent binding constant ($K_a$) and the relaxivity of the adduct ($r_{1b}$) were determined by measuring $R_1$ values of the complex (0.32 mM for **Fe1** and 0.47 mM for **Fe2**) as a function of increasing HSA concentration (0.05 to 2.0 mM) in PBS at pH 7.4, 25 °Cand 21.5 MHz (Fig. 6C in the manuscript)). The number of binding sites was identified through the relaxometric titration of HSA solutions, at a fixed concentration of 0.1 mM, with increasing concentrations of **Fe1** or **Fe2** (0.02 to 4.5 mM) (Fig. 6D in the manuscript).

**HSA-Fe2 binding by fluorescence spectroscopy**

To corroborate the HSA binding results from PRE studies, fluorescence spectroscopy was used to determine the **Fe2**-HSA binding constant ($K_a$). The protein interaction study was performed by tryptophan fluorescence quenching experiments using HSA (2 $\mu$M) in PBS (pH 7.4) containing 15% DMF. Quenching of the emission intensity of tryptophan residue (Trp214) of HSA at 348 nm (excitation wavelength at 285 nm) was monitored using **Fe2** as the quencher by gradually increasing the concentration (5 to 40 $\mu$M).[14] A double-logarithmic plot was constructed based on the equation: $\log [(F_o - F)/F] = \log K_a + n \log$ [**Fe2**], where $F_o$ and $F$ are the respective fluorescent intensity in the absence and presence of **Fe2** and $n$ is the binding site (Ref. 63 in the manuscript). The values of $K_a$ were obtained using GraphPad Prism 10 software.

**NMRD profiles**

NMRD profiles were obtained using a Stelar SpinMaster FFC NMR relaxometer at a continuum of proton frequencies from 0.01 to 10 MHz. Additional data in the 20–80 MHz frequency range were obtained with a Bruker WP80 electromagnet coupled to a Stelar SpinMaster spectrometer both equipped with a Stelar VTC-91 for temperature control. The temperature inside the probe was checked with a calibrated RS PRO RS55-11 digital thermometer. Aqueous and HSA solutions of the complex were measured at 25 °C.

**$^{17}$O-$R_2$-NMR measurements**

$^{17}$O-NMR measurements were recorded at 14.1 T on a Bruker Avance 600 spectrometer at variable temperature. $D_2O$ capillary was used for sample locking. Samples contained 1% of $H_2{}^{17}O$ (Cambridge Isotope) and the complex (20.0 mM **Fe1** or **Fe2**, 20.0 mM $[Fe(DTPA)]^{2-}$ and 4.5 mM $[Fe(CDTA)]^{-}$). The width at half-maximum ($\Delta\omega_{dia}$) of the $H_2{}^{17}O$ signal in pure water was determined over the investigated temperature range and subtracted from the width at half-maximum ($\Delta\omega_{Fe}$) of the test solution containing the complex. The transverse relaxation rate ($R_2$) was calculated as follows: $R_2 = \pi[\Delta\omega_{Fe} - \Delta\omega_{dia}]$. To compare the different profiles, $R_2$ values were normalized to 20.0 mM concentration of the complex.

**MRI phantom imaging with Fe2**

MRI phantom images were acquired at room temperature (*ca*. 21°C) using a 7.1 T Bruker Avance Neo 300 MHz spectrometer equipped with a 2.5 microimaging probe. $T_1$ weighted images were obtained using a standard multislice multiecho sequence (MSME) with the following parameters: TR = 250 ms, TE = 3.3 s, FOV = 3 cm × 3 cm, slice thickness = 1 mm, matrix size 128 × 128. $T_2$-weighted images (not shown) were acquired using a standard Rapid Acquisition with Refocused Echoes (RARE) sequence with the following parameters: TR = 4000 ms, TE = 5.5 s, FOV = 3 cm × 3 cm, slice thickness = 1 mm, RARE factor = 32, matrix size 128 × 128.

## Schemes, Figures, Tables, and Plots

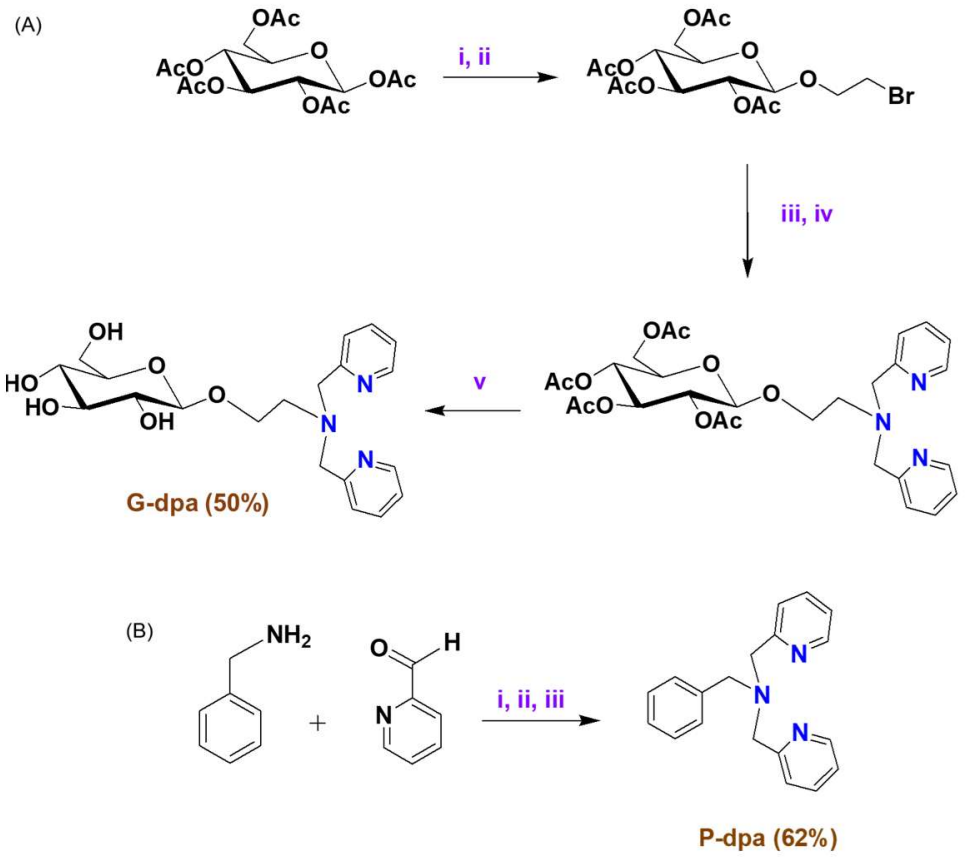


**Scheme S1.** (A) Steps showing the synthesis of G-dpa ligand. Reagents and conditions: (i) 2-bromoethnaol, (ii) $BF_3.Et_2O$ in DCM ($N_2$ atm); (iii) di-2-picolylamine, (iv) $K_2CO_3$ in DMF (3 days at room temperature); (v) NaOMe/MeOH (DOWEX-$8H^+$ resin). (B) Steps showing the synthesis of P-dpa ligand. Reagents and conditions: (i) Sodium triacetoxyborohydride in DCM, (ii) NaH, (iii) HCl.

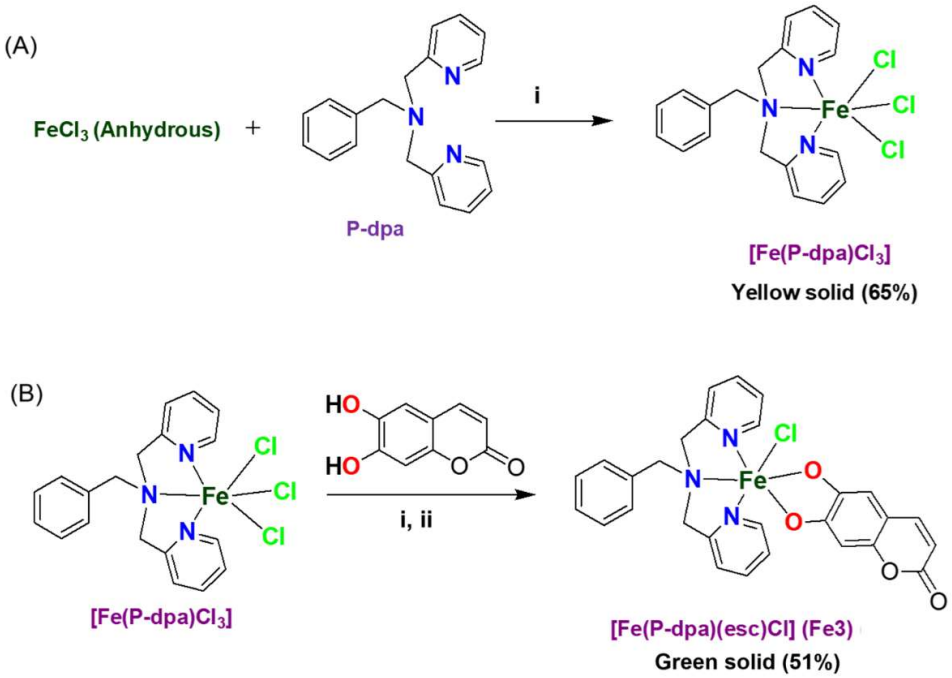


**Scheme S2.** (A) Synthesis of the phenyl-conjugated precursor [Fe(P-dpa)$Cl_3$] (i = Anhydrous MeOH). (B) Synthesis of [Fe(P-dpa)(esc)Cl] (**Fe3**) (i = 2 equiv. $Et_3N$, ii = Anhydrous MeOH).

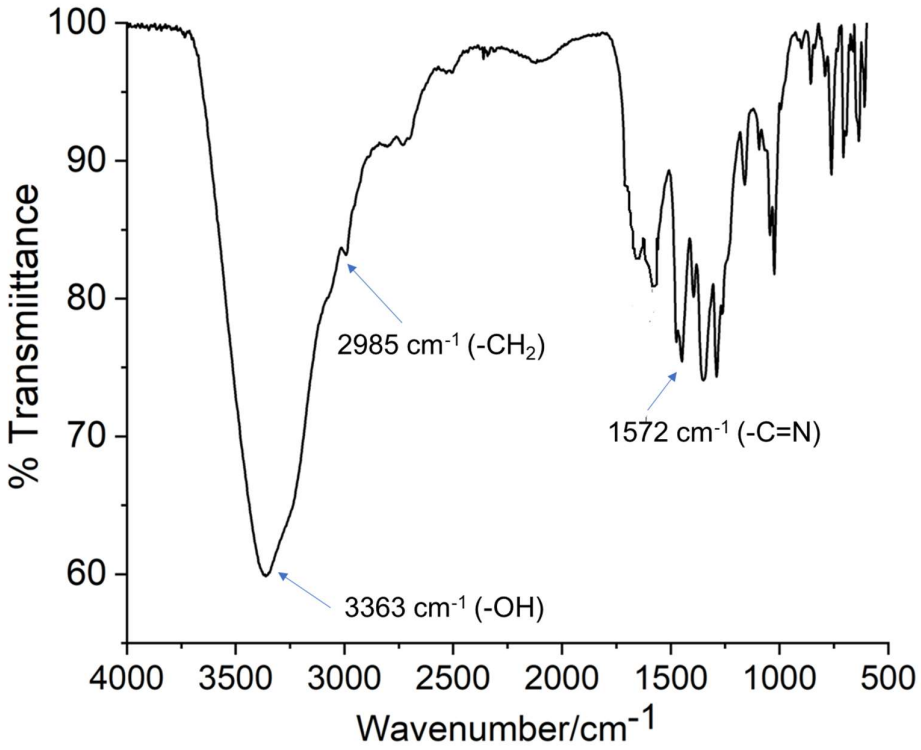


**Fig. S1.** Solid-state FT-IR spectrum of complex **Fe1**.

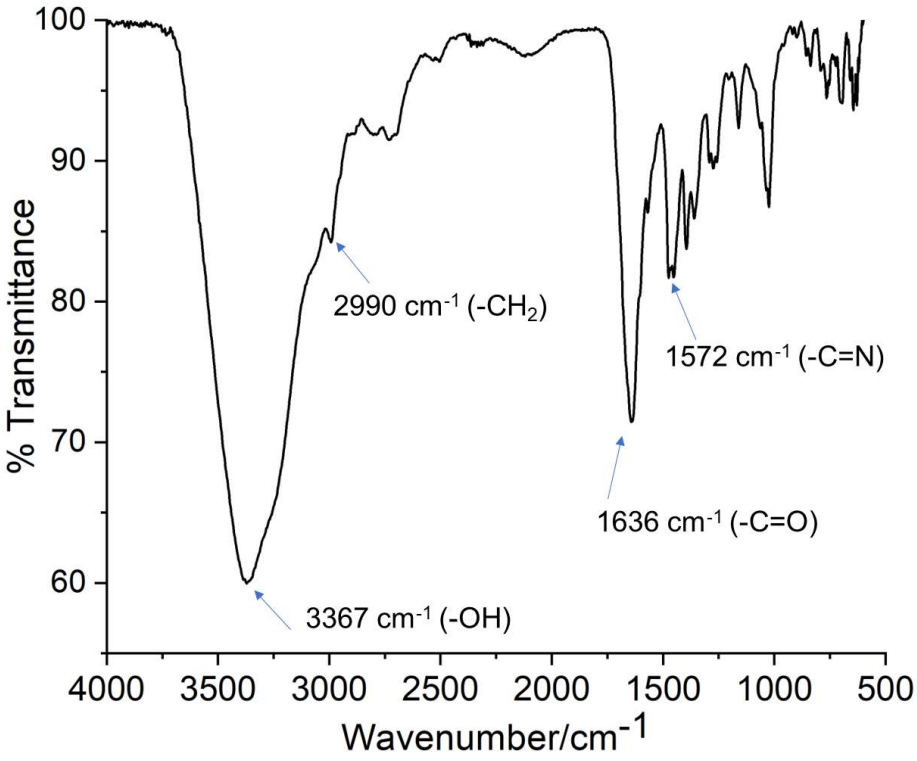


**Fig. S2.** Solid-state FT-IR spectrum of complex **Fe2**.

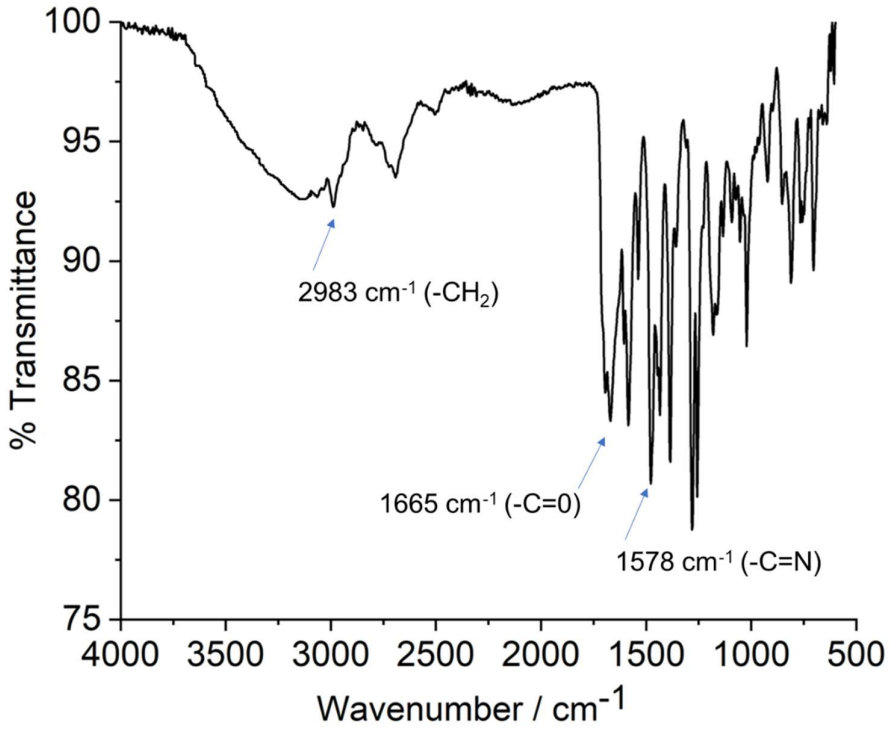


**Fig. S3.** Solid-state FT-IR spectrum of complex **Fe3**.

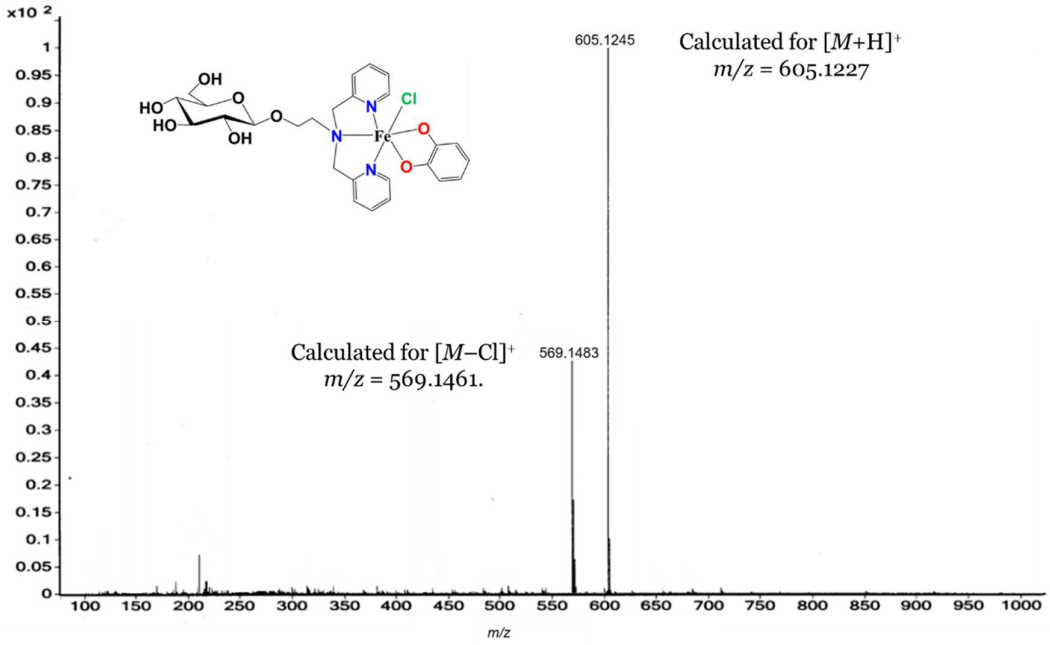


**Fig. S4.** ESI-HRMS (+) spectrum of **Fe1** in MeOH/$H_2O$ (19:1 v/v).

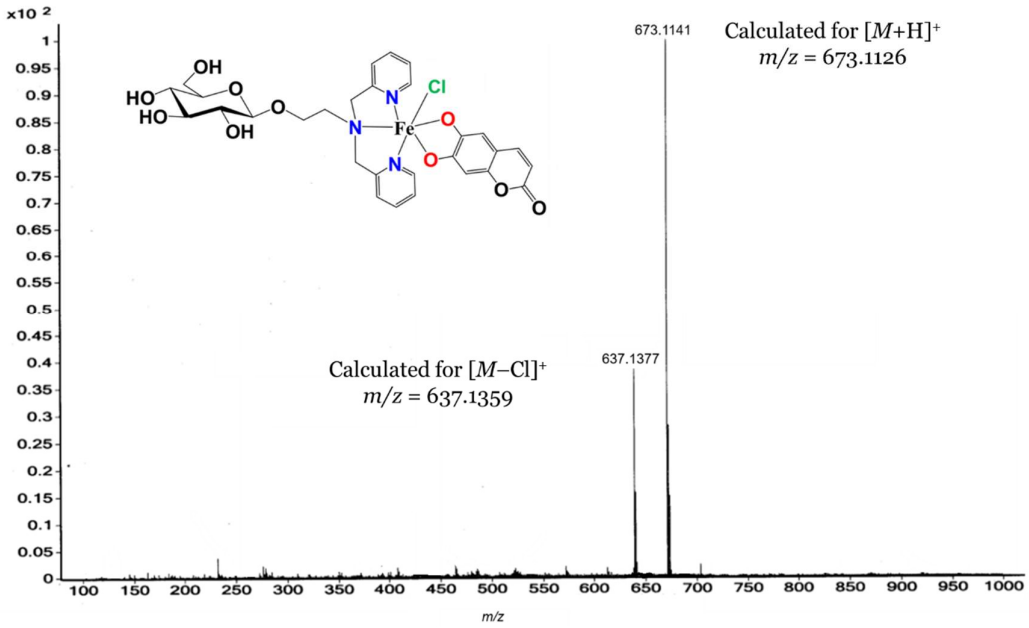


**Fig. S5.** ESI-HRMS (+) spectrum of **Fe2** in MeOH/$H_2O$ (19:1 v/v).

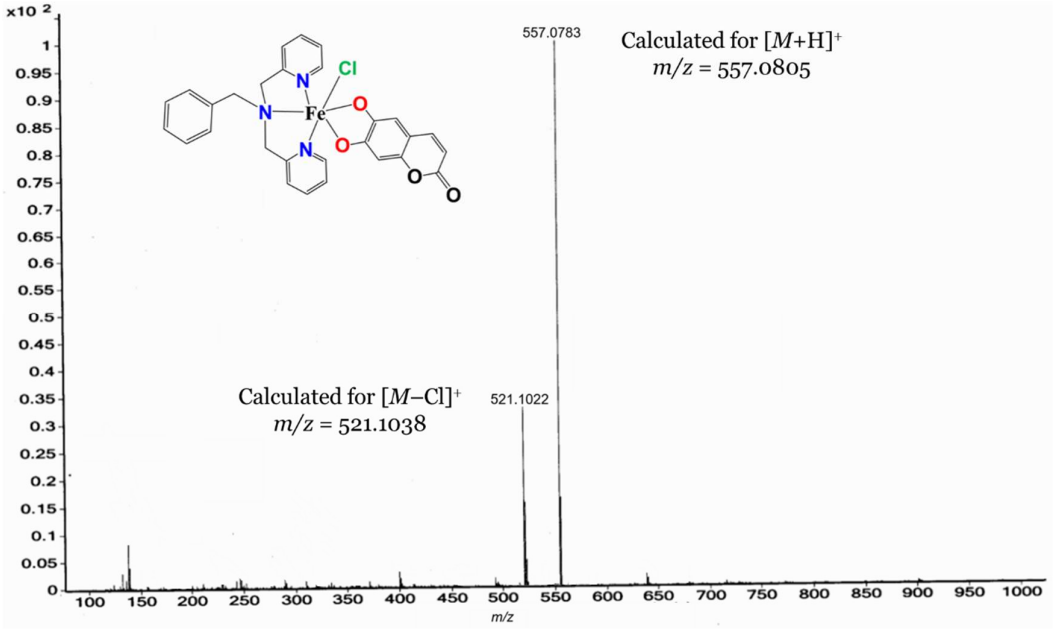


**Fig. S6.** ESI-HRMS (+) spectrum of **Fe3** in MeOH/$H_2O$ (19:1 v/v).

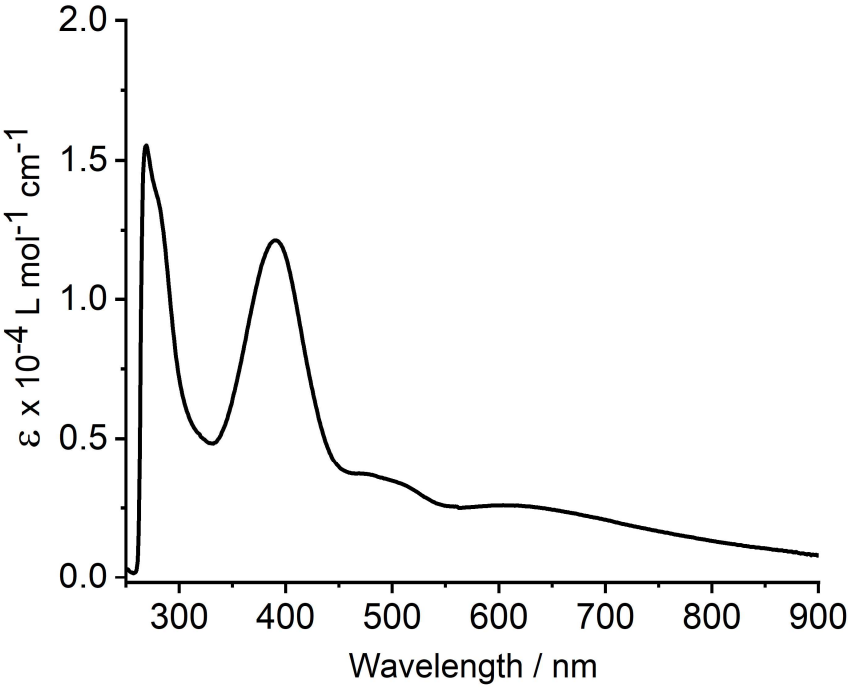


**Fig. S7.** UV-visible spectrum of **Fe3** (75 $\mu$M) acquired at room temperature in PBS (pH 7.4) solution.

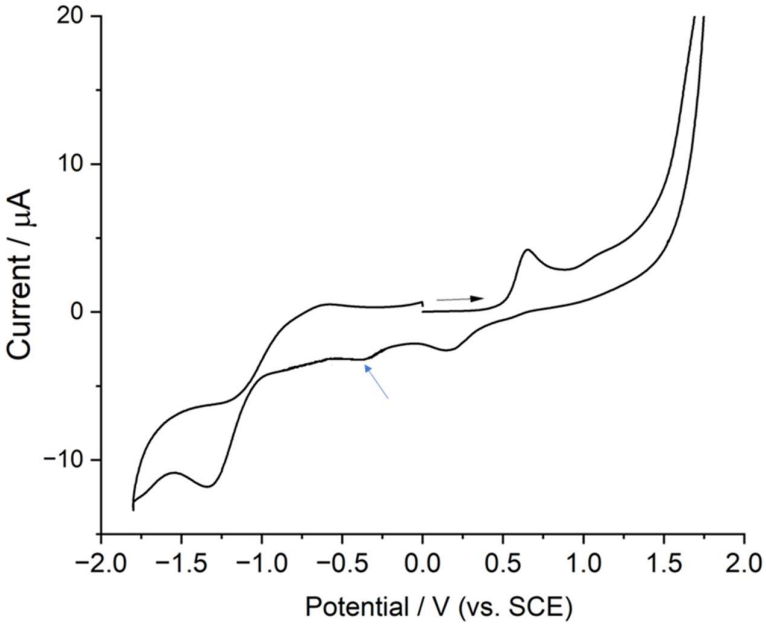


**Fig. S8.** Cyclic voltammograms of **Fe1** (2.0 mM, 25°C) in a DMF/PBS [9:1 (v/v)] solution. The voltammograms were recorded with added (0.1 M) tetrabutylammonium perchlorate (TBAP) as the supporting electrolyte (scan rate = 100 mV/s). The blue arrow represents the Fe(III)/Fe(II) redox potential. The redox waves seen at +0.25 V could be due to catecholate to semiquinone oxidation. The potential at -1.20 V could be due to dipicolylamine-based redox responses.

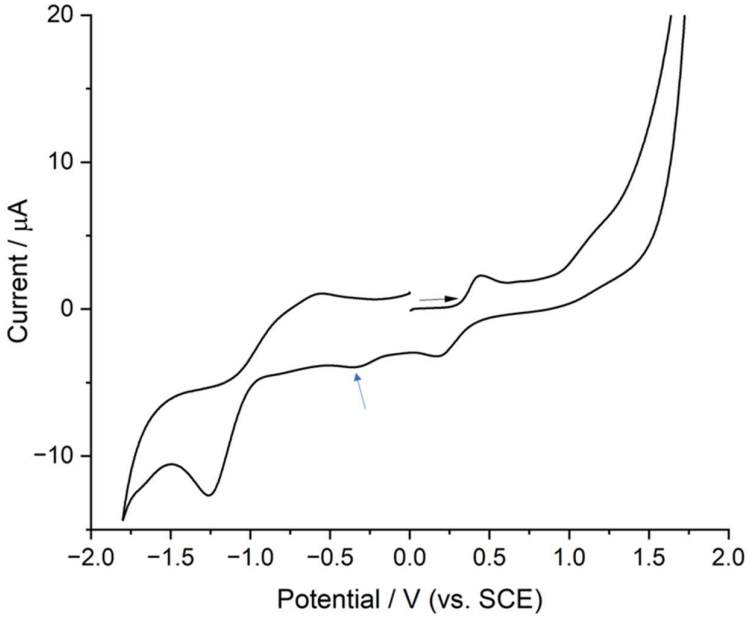


**Fig. S9.** Cyclic voltammograms of **Fe2** (2.0 mM, 25°C) in a DMF/PBS [9:1 (v/v)] solution. The voltammograms were recorded with added (0.1 M) tetrabutylammonium perchlorate (TBAP) as the supporting electrolyte (scan rate = 100 mV/s). The blue arrow represents the Fe(III)/Fe(II) redox potential. The redox waves seen at +0.25 V could be due to catecholate to semiquinone oxidation. The potential at -1.20 V could be due to dipicolylamine-based redox responses.

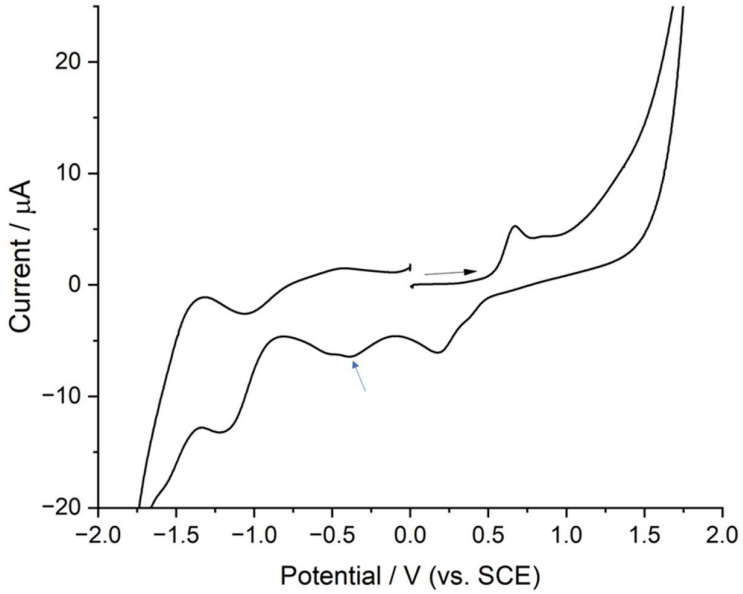


**Fig. S10.** Cyclic voltammograms of **Fe3** (2.0 mM, 25°C) in a DMF/PBS [9:1 (v/v)] solution. The voltammograms were recorded with added (0.1 M) tetrabutylammonium perchlorate (TBAP) as the supporting electrolyte (scan rate = 100 mV/s). The blue arrow represents the Fe(III)/Fe(II) redox potential. The redox waves seen at +0.25 V could be due to catecholate to semiquinone oxidation. The potential at -1.20 V could be due to dipicolylamine-based redox responses.

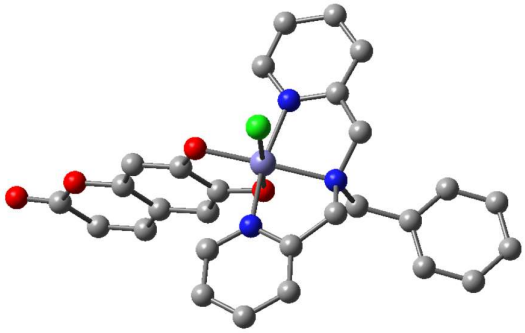

**Fig. S11.** DFT optimized structure of **Fe3**. Atom representation: C (gray), N (blue); O (red); Cl (green); Fe (light blue).

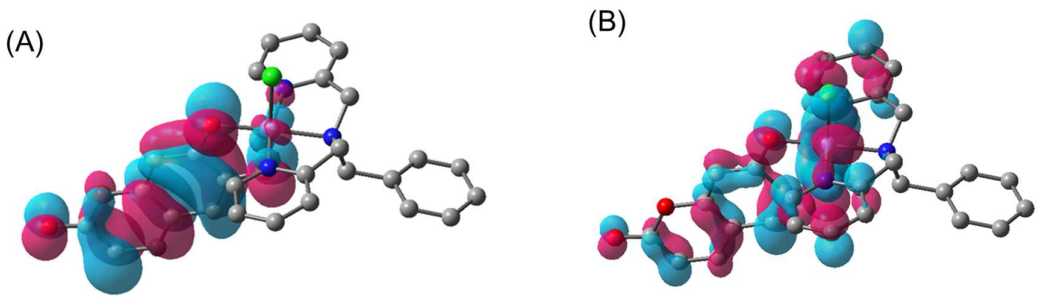


**Fig. S12.** (A) HOMO and (B) LUMO of **Fe3** as determined from the DFT calculations. Atom representation: C (gray), N (blue); O (red); Cl (green); Fe (light blue).

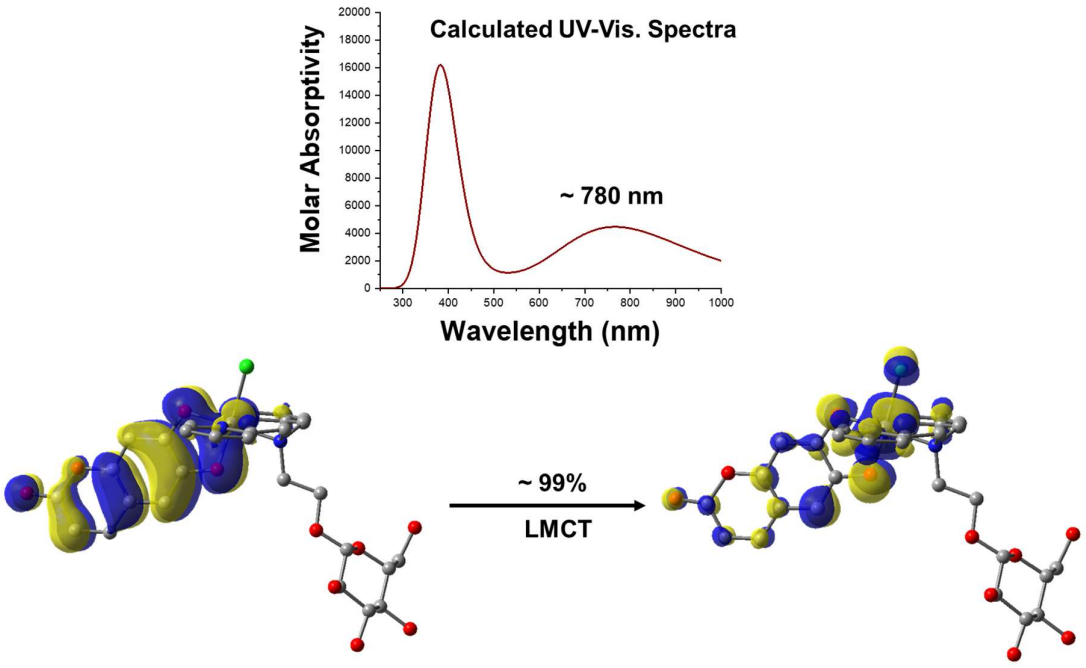


**Fig. S13.** Natural transition orbitals (NTOs) of **Fe2** involved in the charge-transfer electronic transitions predicted at 780 nm (164B to 165B) from the TD-DFT calculations. For comparison, the experimental spectrum of **Fe2** is also shown. Atom representation: C (gray), N (blue); O (red); Cl (green); Fe (light blue).

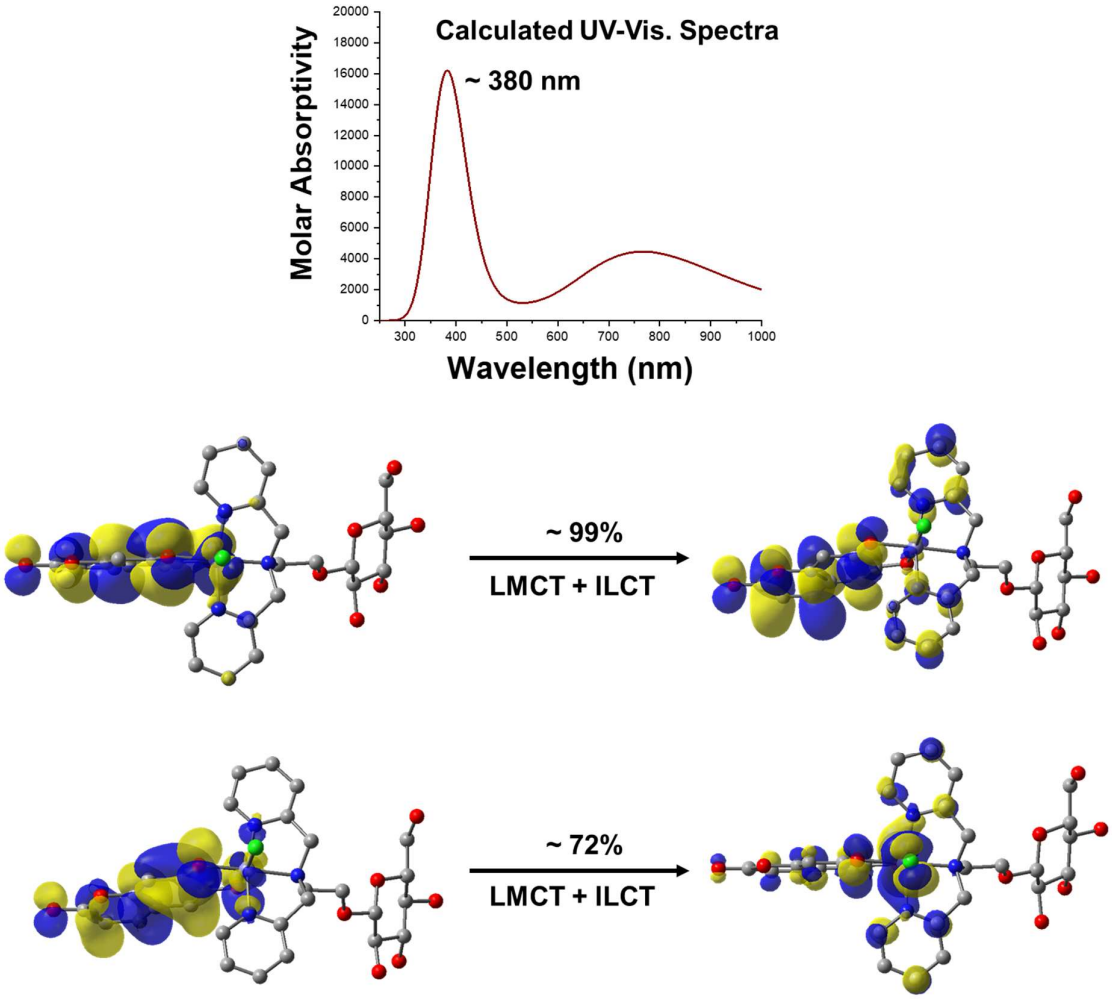


**Fig. S14.** Natural transition orbitals (NTOs) of **Fe2** involved in the charge-transfer electronic transitions predicted at 380 nm (164B to 166B) from the TD-DFT calculations. For comparison, the experimental spectrum of **Fe2** is also shown. Atom representation: C (gray), N (blue); O (red); Cl (green); Fe (light blue).

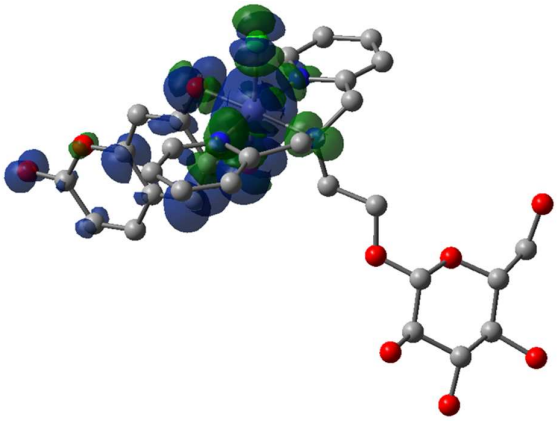

**Fig. S15.** Spin density calculations on **Fe2** employing the TD-UB3LYP/LANL2DZ method and using the TD-DFT calculations.

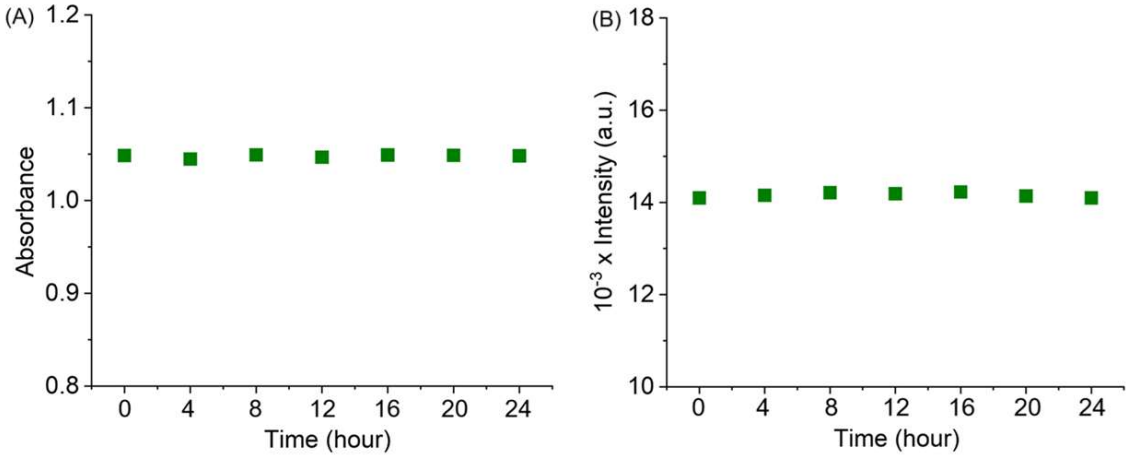


**Fig. S16.** Stability studies showing the plots of the time-dependent changes in the absorbance of the band at 725 nm in the UV-visible spectra (in panel A, 255 μM) and in the emission intensity of the band at 522 nm in the emission spectra (in panel B, 85 μM) of **Fe2**, taken at 4-hour intervals (0, 4, 8, 12, 16, 20, and 24 hours) up to 24 hours. All spectra were acquired at 25°C in DMEM (pH 7.4).

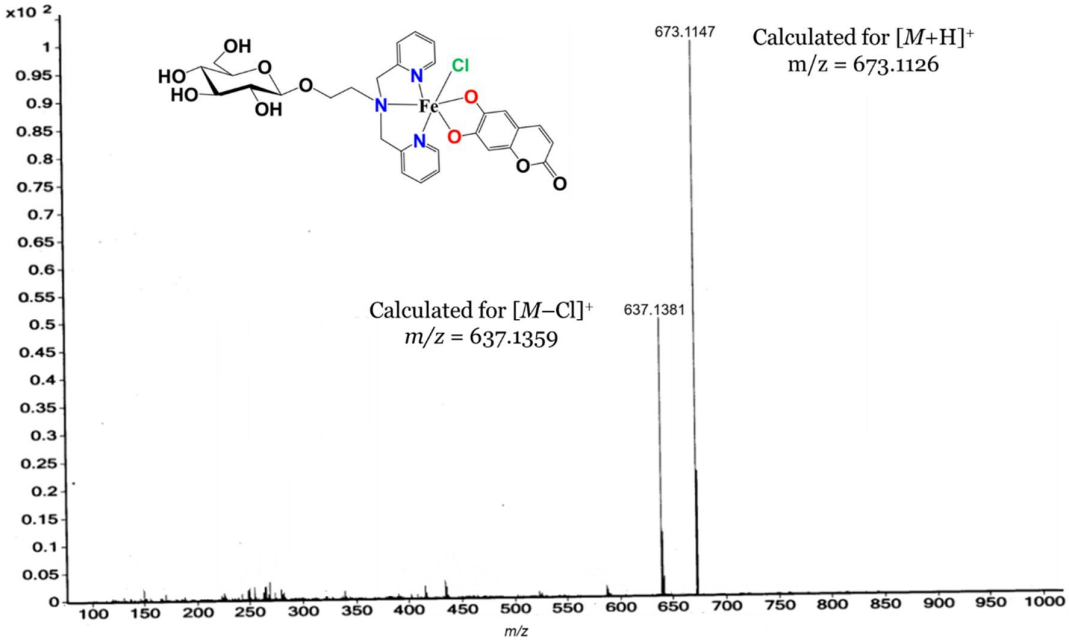


**Fig. S17.** ESI-HRMS (+) spectrum of **Fe2** recorded in MeOH/$H_2O$ (19:1 v/v) after 24 h of dark incubation.

**Table S1.** $IC_{50}$ values (in $\mu$M units) of complexes **Fe2** and **Fe3** across various glucose concentrations and in the presence of GLUT-1 inhibitors.

| Complex | Cell Line | 2 h (5.0 mM)[a] | 4 h (5.0 mM)[a] | 2 h (1.0 mM) | 2 h (10.0 mM) | 2 h (5.0 mM[a] +EDG) | 2 h (5.0 mM[a] + WZB-117) |
|---|---|---|---|---|---|---|---|
| **Fe2** | HeLa | 14.1 ± 0.4 | 13.5 ± 0.2 | 9.7 ± 0.3 | 83.5 ± 2.7 | 51.8 ± 2.0 | 64.4 ± 2.1 |
| **Fe2** | MCF-7 | 9.2 ± 0.3 | 8.6 ± 0.2 | 5.5 ± 0.1 | 63.7 ± 2.1 | 35.3 ± 1.5 | 48.4 ± 1.8 |
| **Fe3** | HeLa | 21.3 ± 0.7 | 15.6 ± 0.5 | 20.8 ± 0.8 | 21.7 ± 0.7 | n.d. | 21.8 ± 0.3 |
| **Fe3** | MCF-7 | 15.8 ± 0.4 | 10.8 ± 0.3 | 15.5 ± 0.5 | 15.2 ± 0.2 | n.d. | 15.1 ± 0.4 |

[a] Refers to standard glucose concentration in the culture media. All experiments used red light (600–720 nm, 50 J $cm^{-2}$, 15 minutes). n.d.: Not determined.

**Table S2.** Fe contents (ng per $10^6$ cells) of **Fe2** and **Fe3** across various glucose concentrations and in the presence of GLUT-1 inhibitor WZB-117 as determined from the ICP-MS analysis.

| Complex | Cell Line | 2 h (5.0 mM)[a] | 4 h (5.0 mM) | 2 h (1.0 mM) | 2 h (10.0 mM) | 2 h (5.0 mM[a] + WZB-117) |
|---|---|---|---|---|---|---|
| **Fe2** | HeLa | 64.3 ± 3.2 | 67.1 ± 3.2 | 88.6 ± 3.1 | 23.3 ± 2.2 | 38.3 ± 2.7 |
| **Fe2** | MCF-7 | 105.5 ± 3.5 | 107.7 ± 3.4 | 127.5 ± 3.7 | 57.5 ± 3.3 | 77.5 ± 3.4 |
| **Fe3** | HeLa | 40.1 ± 2.6 | 62.3 ± 3.1 | 41.2 ± 2.5 | 39.4 ± 2.0 | 40.7 ± 1.9 |
| **Fe3** | MCF-7 | 71.5 ± 3.4 | 93.4 ± 3.0 | 71.9 ± 3.3 | 72.1 ± 3.6 | 70.7 ± 2.9 |

[a] Refers to standard glucose concentration in the culture media.

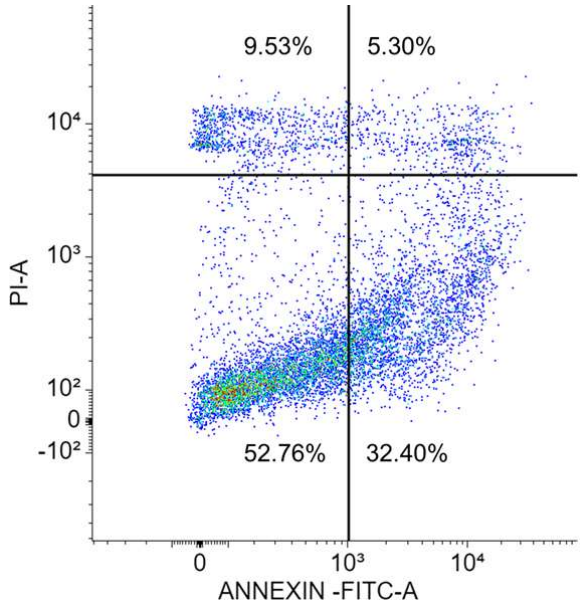


**Fig. S18.** (A) Annexin V-FITC/PI coupled flow cytometric analysis of **Fe2** (15 μM)-treated HeLa cells under red light irradiation (600–720 nm, 50 J $cm^{-2}$, 15 minutes).

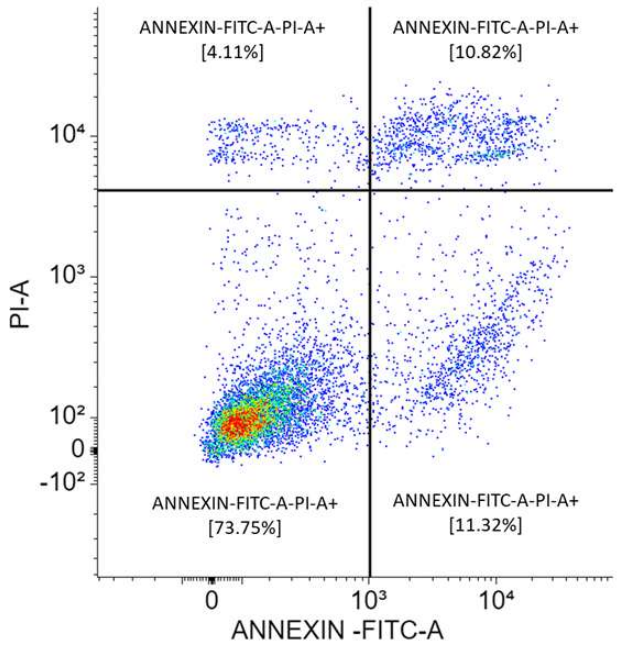


**Fig. S19.** Annexin V-FITC/PI coupled flow cytometric analysis of **Fe2** (15 μM)-treated HeLa cells under dark conditions.

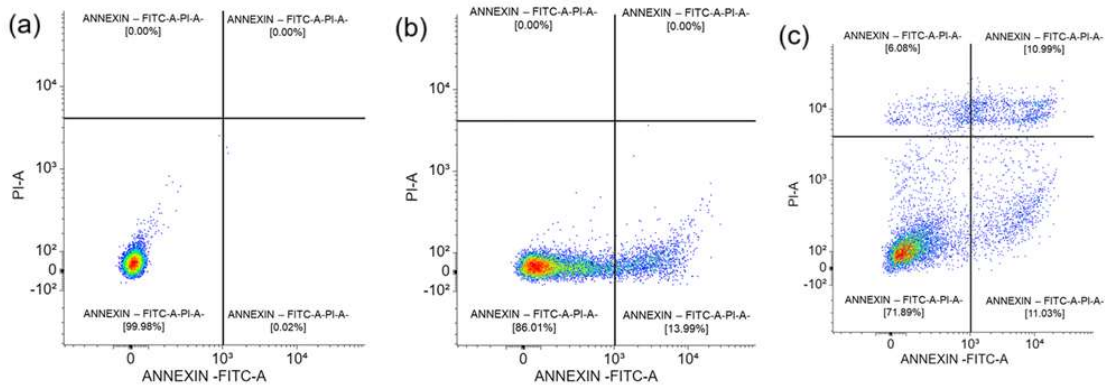


**Fig. S20.** Annexin V-FITC/PI coupled flow cytometric analysis showing various controls with HeLa cells: (a) Cells only; (b) Cells + Annexin-V-FITC only; (c) Cells + Annexin-V-FITC + PI. (PI = propidium iodide). These controls are reproduced with permission from Ref. 15. Copyright 2024 Royal Society of Chemistry.

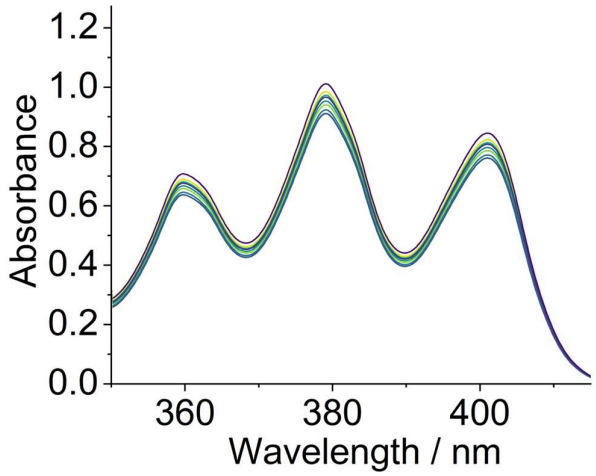


**Fig. S21.** (C) The UV-visible spectra of ABDA (12 μM), treated with **Fe2** (20 $\mu$M) in the presence of $NaN_3$ (10.0 mM) and acquired every 2 minutes (0, 2, 4, 6, 8, 10, 12, 14, 16, 18, and 20 minutes) during continuous irradiation for up to 20 minutes.

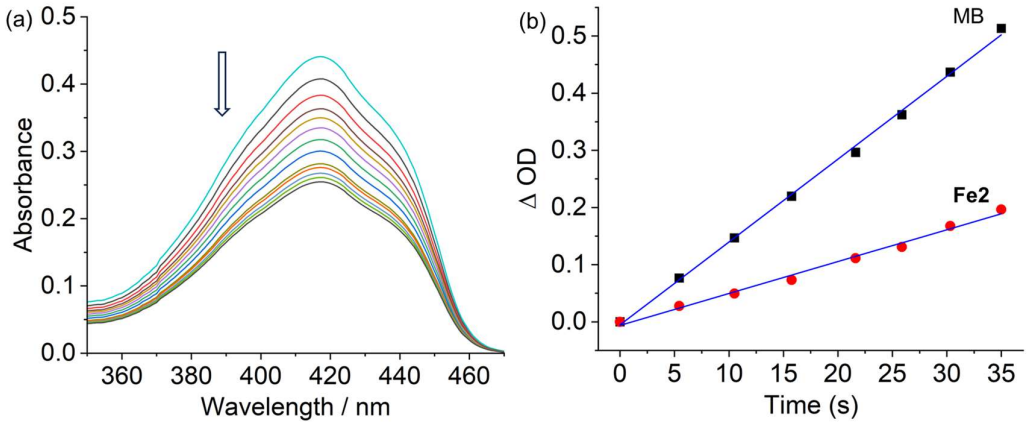


**Fig. S22.** (a) The gradual drop (indicated by the down-pointing arrow) in the absorbance of 1,3-diphenylisobenzofuran (DPBF) treated with **Fe2** (15 $\mu$M) under light irradiated conditions. The spectra were acquired at 5 s intervals up to 60 s (0 to 60 s). (b) Plots of ΔOD (optical density) vs. time (s) to calculate singlet oxygen quantum yield ($\phi_\Delta$) for **Fe2** (filled red circle). Methylene blue (MB, filled black square) was used as a reference. All experiments used a red laser light (705 nm, 38 mW) for irradiation at 25°C.

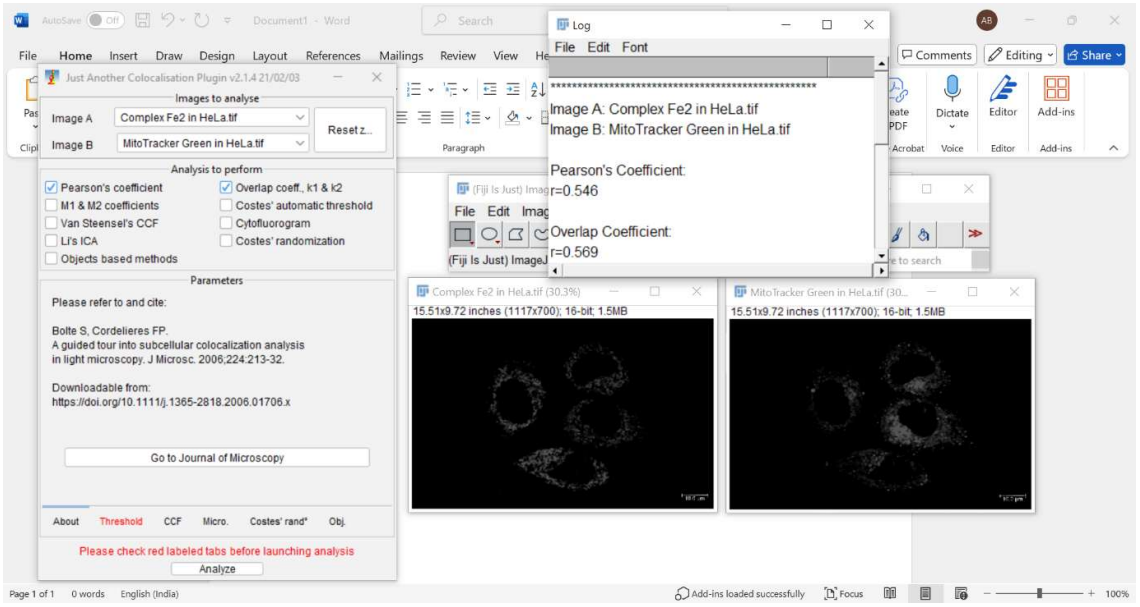


**Fig. S23.** Calculation of Pearson Coefficient (PC) and Operlap Coefficient (OC) for confocal images for **Fe2** and MitTracker green (MTG) in HeLa cells using ImageJ software with JACoP plugin.

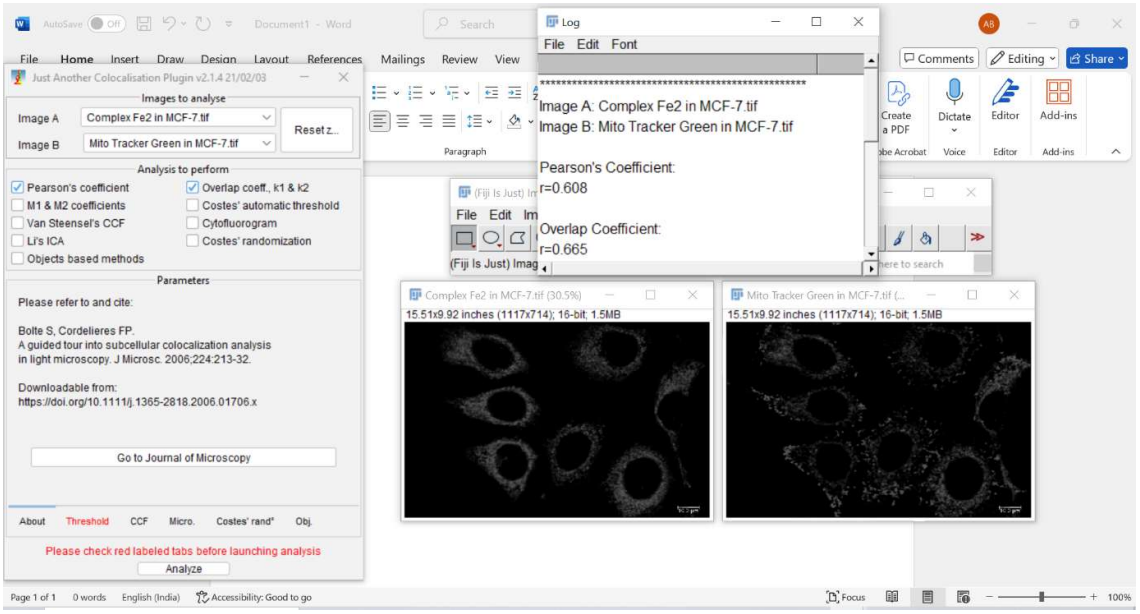


**Fig. S24.** Calculation of Pearson Coefficient (PC) and Operlap Coefficient (OC) for confocal images for **Fe2** and MitTracker green (MTG) in MCF-7 cells using ImageJ software with JACoP plugin.

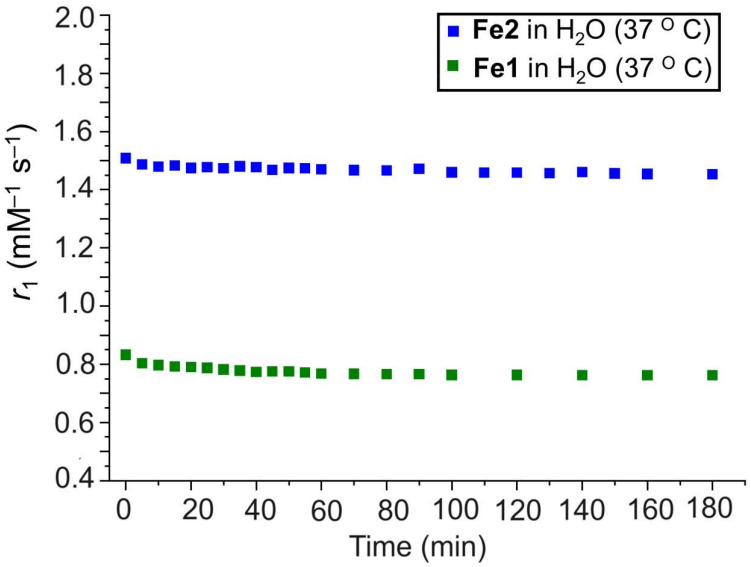


**Fig. S25.** Variation of the proton longitudinal millimolar relaxivities of **Fe1** and **Fe2** measured in pure $H_2O$ at 21.5 MHz and 37°C for 3 hours.

## References


1. D. D. Perrin, W. L. F. Armarego and D. R. Perrin, *Purification of Laboratory Chemicals*, Pergamon Press: Oxford, **1980**.
2. N. M. F. Carvalho, A. Horn Jr., A. J. Bortoluzzi, V. Drago and O. A. C. Antunes, *Inorg. Chim. Acta*, 2006, **359**, 90–98.
3. J.-F. Li and Q.-Y. Chen, *Spectrochim. Acta Part A*, 2009, **73**, 25–28.
4. (a) D. F. Evans, *J. Chem. Soc.*, 1961, 1987; (b) D. F. Evans, *J. Chem. Soc.,* 1959, 2003–2005.
5. M. J. Frisch, G. W. Trucks, H. B. Schlegel, G. E. Scuseria, M. A. Robb, J. R. Cheeseman, G. Scalmani, V. Barone, G. A. Petersson, H. Nakatsuji, X. Li, M. Caricato, A. V. Marenich, J. Bloino, B. G. Janesko, R. Gomperts, B. Mennucci, H. P. Hratchian, J. V. Ortiz, A. F. Izmaylov, J. L. Sonnenberg, D. Williams-Young, F. Ding, F. Lipparini, F. Egidi, J. Goings, B. Peng, A. Petrone, T. Henderson, D. Ranasinghe, V. G. Zakrzewski, J. Gao, N. Rega, G. Zheng, W. Liang, M. Hada, M. Ehara, K. Toyota, R. Fukuda, J. Hasegawa, M. Ishida, T. Nakajima, Y. Honda, O. Kitao, H. Nakai, T. Vreven, K. Throssell, J. A. Montgomery, Jr., J. E. Peralta, F. Ogliaro, M. J. Bearpark, J. J. Heyd, E. N. Brothers, K. N. Kudin, V. N. Staroverov, T. A. Keith, R. Kobayashi, J. Normand, K. Raghavachari, A. P. Rendell, J. C. Burant, S. S. Iyengar, J. Tomasi, M. Cossi, J. M. Millam, M. Klene, C. Adamo, R. Cammi, J. W. Ochterski, R. L. Martin, K. Morokuma, O. Farkas, J. B. Foresman and D. J. Fox. Gaussian 16, revision C.01. Gaussian, Inc., Wallingford CT, 2016.
6. G., II Jones, J. R. Jackson, C. Choi and W. R. Bergmark, *J. Phys. Chem.,* 1985, **89**, 294−300.
7. (a) J. R. Lakowicz, in *Principles of Fluorescence Spectroscopy* (Kluwer Academic/Plenum Publishers, New York, 1999; (b) A. T. R. Williams, S. A. Winfield and J. N. Miller, *Analyst,* 1983, **108**, 1067−1071.

8. J. Wu, D. G. J. Goodwin, K. Peter, D. Benoit, W. Li, D. H. Fairbrother and J. D. Fortner, *Environ., Sci. Technol. Lett.,* 2014, **1**, 490–494.
9. T. Mosmann, *J. Immunol. Methods,* 1983, **65**, 55–63.
10. T. N. Aslan, E. Aşık, N. T. Güray and M. Volkan, *J. Biol. Inorg. Chem.,* 2020, **25**, 1139–1152.
11. J. L. McClintock and B. P. Ceresa, *Invest. Opthalmol. Vis. Sci.,* 2010, **51**, 3455–3461.
12. T. Takanashi, Y. Ogura, H. Taguchi, M. Hashizoe and Y. Honda, *Invest. Ophthalmol. Vis. Sci.,* 1997, **38**, 2721–2728.
13. Y. Svenskaya, F. Garello, E. Lengert, A. Kozlova, R. Verkhovskii, V. Bitonto, M. R. Ruggiero, S. German, D. Gorin and E. Terreno, *Nanotheranostics,* 2021, **5**, 362−377.
14. N. S. Quiming, R. B. Vergel, M. G. Nicolas and J. A. Villanueva, *J. Health Sci.,* 2005**, 51**, 8–15.
15. B. Deka, T. Sarkar, A. Bhattacharyya, R. J. Butcher, S. Banerjee, S. Deka, K. K. Saikia and A. Hussain, *Dalton Trans.*, 2024, **53**, 4952–4961.